FORM TI-12
12/97

WAPD-T-3252

RECEIVED
FEB 08 1999
OSTI

IRRECOVERABLE PRESSURE LOSS COEFFICIENTS FOR TWO OUT-OF-PLANE PIPING ELBOWS AT HIGH REYNOLDS NUMBER

R. D. Coffield
R. B. Hammond
P. T. McKeown

DE-AC11-93PN38195

NOTICE

This report was prepared as an account of work sponsored by the United States Government. Neither the United States, nor the United States Department of Energy, nor any of their employees, nor any of their contractors, subcontractors, or their employees, makes any warranty, express or implied, or assumes any legal liability or responsibility for the accuracy, completeness or usefulness of any information, apparatus, product or process disclosed, or represents that its use would not infringe privately owned rights.

BETTIS ATOMIC POWER LABORATORY WEST MIFFLIN, PENNSYLVANIA 15122-0079

Operated for the U.S. Department of Energy
by WESTINGHOUSE ELECTRIC COMPANY,
a division of CBS Corporation

THIS PAGE INTENTIONALLY BLANK

DISCLAIMER

Portions of this document may be illegible in electronic image products. Images are produced from the best available original document.

IRRECOVERABLE PRESSURE LOSS COEFFICIENTS FOR TWO OUT-OF-PLANE ELBOWS AT HIGH REYNOLDS NUMBERS

ABSTRACT

Pressure drops of multiple piping elbows were experimentally determined for high Reynolds number flows. The testing described has been performed in order to reduce uncertainties in the currently used methods for predicting irrecoverable pressure losses and also to provide a qualification database for computational fluid dynamics (CFD) computer codes. The earlier high Reynolds number correlations had been based on extrapolations over several orders of magnitude in Reynolds number from where the original database existed. Recent single elbow test data shows about a factor of two lower elbow pressure loss coefficient (at 40 x 10^6 Reynolds number) than those from current correlations. This single piping elbow data has been extended in this study to a multiple elbow configuration of two elbows that are 90° out-of-plane relative to each other. The effects of separation distance and Reynolds number have been correlated and presented in a form that can be used for design application. Contrary to earlier extrapolations from low Reynolds numbers (Re < 1.0 x 10^6), a strong Reynolds number dependence was found to exist. The combination of the high Reynolds number single elbow data with the multiple elbow interaction effects measured in this study shows that earlier design correlations are conservative by significant margins at high Reynolds numbers. Qualification of CFD predictions with this new high Reynolds number database will help guide the need for additional high Reynolds number testing of other piping configurations. The study also included velocity measurements at several positions downstream of the first and second test elbows using an ultrasonic flowmeter. Reasonable agreement after the first test elbow was found relative to flow fields that are known to exist from low Reynolds number visual tests and also from CFD predictions. This data should help to qualify CFD predictions of the three-dimensional flow stream downstream of the second test elbow.

1.0 INTRODUCTION

The purposes of the high Reynolds number testing were:

- to accurately define the irrecoverable pressure loss coefficients for tight radius elbows to high Reynolds numbers, and
- to provide an accurate database for qualifying the irrecoverable pressure loss predictions from Computational Fluid Dynamics (CFD) computer codes.

A comparison of single piping elbow data [for r/D = 1.2 and smooth surface finish which is a combination of the lower Reynolds number (Loop 17) testing reported in Reference (a) and the high Reynolds number data described in Reference (b)] was made with various handbook correlations [References (c) to (g)]. All the correlations were found to be conservative, to varying degrees, for Reynolds numbers greater than 10^5. Discrepancies of these correlations with the data range from less than 40% at a Reynolds number of 10^5 to over 250% at 40 x 10^6 Reynolds number. The objective of this particular test phase was to provide a database for this high Reynolds number region since all the existing correlations had been based on extrapolations of measurements which were several orders of magnitude lower in Reynolds number.

The design optimization need for the new database is particularly important at high Reynolds numbers where the pressure losses set the design requirements for the pumps and other major components. The test data shows about a factor of two lower elbow pressure loss coefficient (at 40 x 10^6 Reynolds number) than had been conservatively assumed for earlier design correlations. The system pressure loss reductions can be reallocated for decreasing pumping power requirements, increased design allotments for other components and/or enabling more compact piping arrangements.

In addition to providing direct piping design data for elbow irrecoverable pressure loss coefficients, another objective of the testing was to provide an accurate database for qualifying the piping pressure loss predictions from Computational Fluid Dynamics (CFD) computer codes. This requires accurate flow field characterization to minimize uncertainties in basic parameters needed for the analyses and for comparisons to the data. The data meets this objective since:

- The inlet velocity profile to the test elbow was confirmed by measurements (Reference (b)) to be that for fully developed, turbulent flow in a straight pipe. It can thus be well defined for the analytical models.

- The straight pipe friction factors used for calculating the elbow irrecoverable pressure loss coefficients are based on data measurements in the inlet tangent pipe that are very consistent over the several orders of magnitude variation in Reynolds numbers and are in good agreement with Princeton University measurements for smooth surface finish testing (Reference (h)).

- Pressure loss measurements from pressure taps in the straight pipe flow region upstream of the elbow to pressure taps selected downstream at a position where the flow had regained its straight pipe flow conditions were very consistent over the several orders of magnitude variation in Reynolds number. Inconsistencies of the type associated with troublesome static wall pressure taps were not detectable.

2.0 TEST CONFIGURATION

Figure 2.1 shows the test configuration. Key components are noted on the figure. All test section piping was made of six inch Schedule 160 carbon steel with an inside diameter of 5.189 inches.

The flow straightener shown as Item Number 1 used 35 holes with approximately a 1.2 inch inside diameter each. The design was found to provide the required flow straightening and to be of sufficiently low pressure loss to not detrimentally impact achieving the high Reynolds numbers needed for the test (as described in Reference (b)).

The venturi shown as Item Number 3 was calibrated by Alden Research Laboratory, Inc. The calibration had less than ±0.25% measurement uncertainty.

The piping reducer shown as Item Number 5 has a total angle of less than 10 degrees which assured no adverse pressure gradients that would cause flow separation effects in the flow field entering the inlet tangent piping.

All piping connections for the test elbow and tangent pipes used Grayloc connecting hubs that were specially developed for this test. Diametral variations relative to the normal tangent pipe were maintained within ±0.005 inches and axial spacing at the connector was limited to less than ±0.005 inches. This arrangement helped assure minimum flow disturbances upstream and downstream of the test elbow.

All pressure taps in the inlet and outlet tangent piping were 0.028 inches in diameter. These were initially drilled to 0.024 inches and then increased in two 0.002 inch increments after the surface finish preparation phases. This two step increase in the pressure tap I.D. from 0.024 to 0.028 inches I.D. was intended to maintain a sharp edge on the holes in order to minimize error in the static wall pressure measurements. Small imperfections on the pressure tap edge can cause either increased pressure readings if the flow is deflected into the tap hole (e.g., rounding of the upstream edge while the downstream edge is square) or a pressure depression if the defect causes localized acceleration of the mainstream (e.g., rounding of the downstream edge while the upstream edge is square).

Four separation distances between the two test elbows (Item Number 7a and 7b) were tested. These distances in piping diameters were:

Configuration	Separation Distance (L_s/D)
No separation pipes	3.16
Short separation pipes	6.16
Long separation pipes	13.66
Long plus short separation pipes	16.66

The vendor produced the smooth surface on the test piping components by a mechanical polishing process. Prior to testing, the piping was passivated at 550°F for ten days. This formed a layer of magnetite (Fe_2O_4) on the surface which helped minimize other types of oxidation like hematite (Fe_2O_3) which could have caused surface pitting. The surface maintained its original surface roughness (prior to passivation) throughout the test period. Magnetite forms an extremely thin equilibrium layer (fractions of a mil) that tenaciously attaches at about the same thickness on all the exposed base metal.

The test instrumentation was configured to provide the following accuracies for measured test parameters:

- Flow rate (combined uncertainties including differential pressure reading and venturi flow coefficients) ±1%
- Differential pressures ±1%
- Water temperature (with thermocouple calibration data incorporated) ±2°F
- Loop pressure ±20 psi

The carbon steel test section piping inside diameter was corrected for thermal expansion effects with the relationship:

$$D = [1 + \alpha(t - t_{meas})]d_{meas}$$

where: t = operating temperature

t_{meas} = temperature that ID was measured (= 70°F)

d_{meas} = measured inside pipe diameter

α = thermal expansion coefficient

The following values were used for the carbon steel thermal expansion coefficient (Reference (b)):

Temperature (°F)	$\alpha \times 10^{-6}$ (in/in/°F)
70	6.07
200	6.38
300	6.60
400	6.82
500	7.02
600	7.23

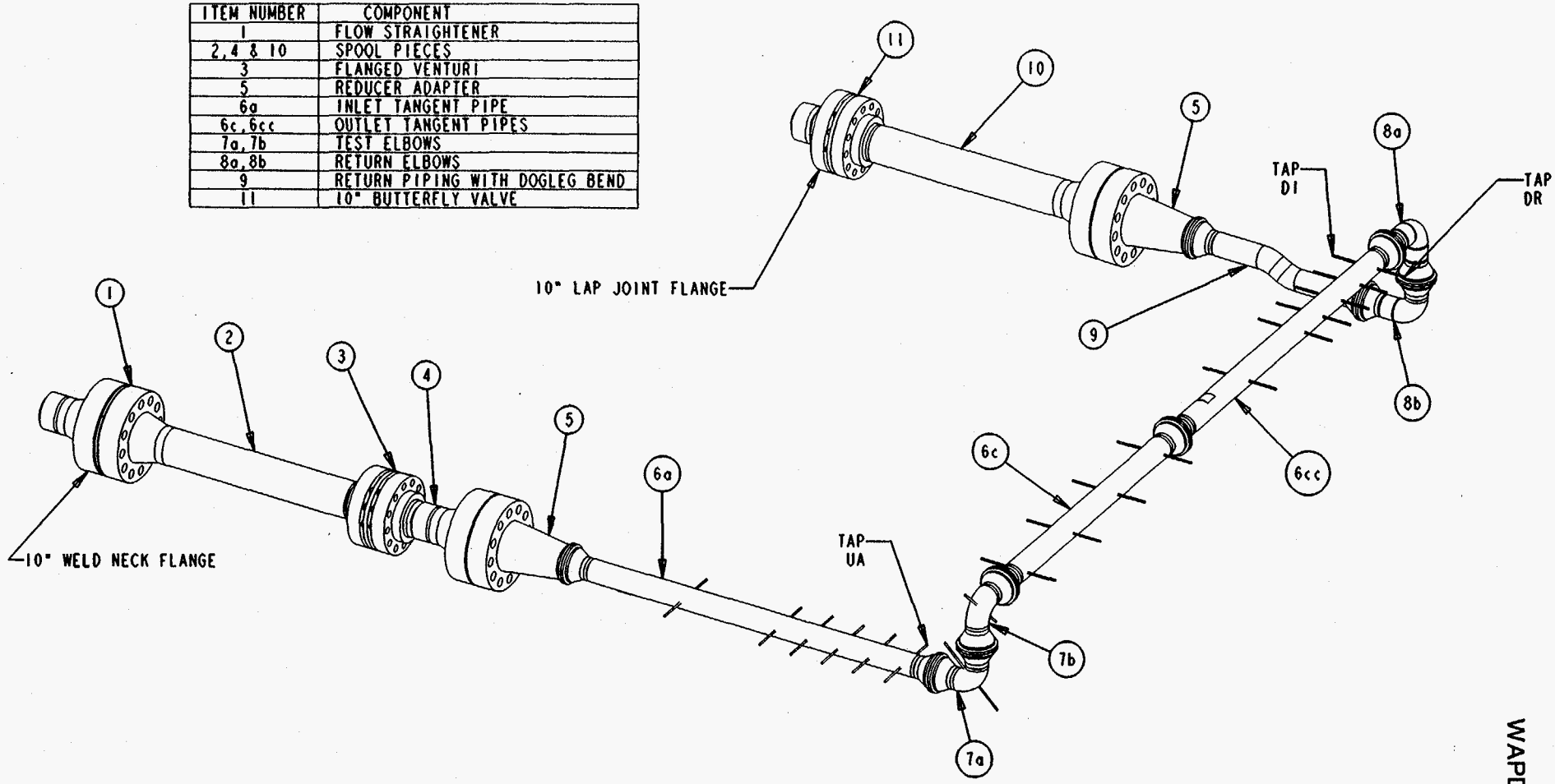

FIGURE 2.1a
Major Components for High Reynolds Number Multiple Elbow Test (With No Separation Pipes, L_s /D= 3.16)

WAPD-T-3252

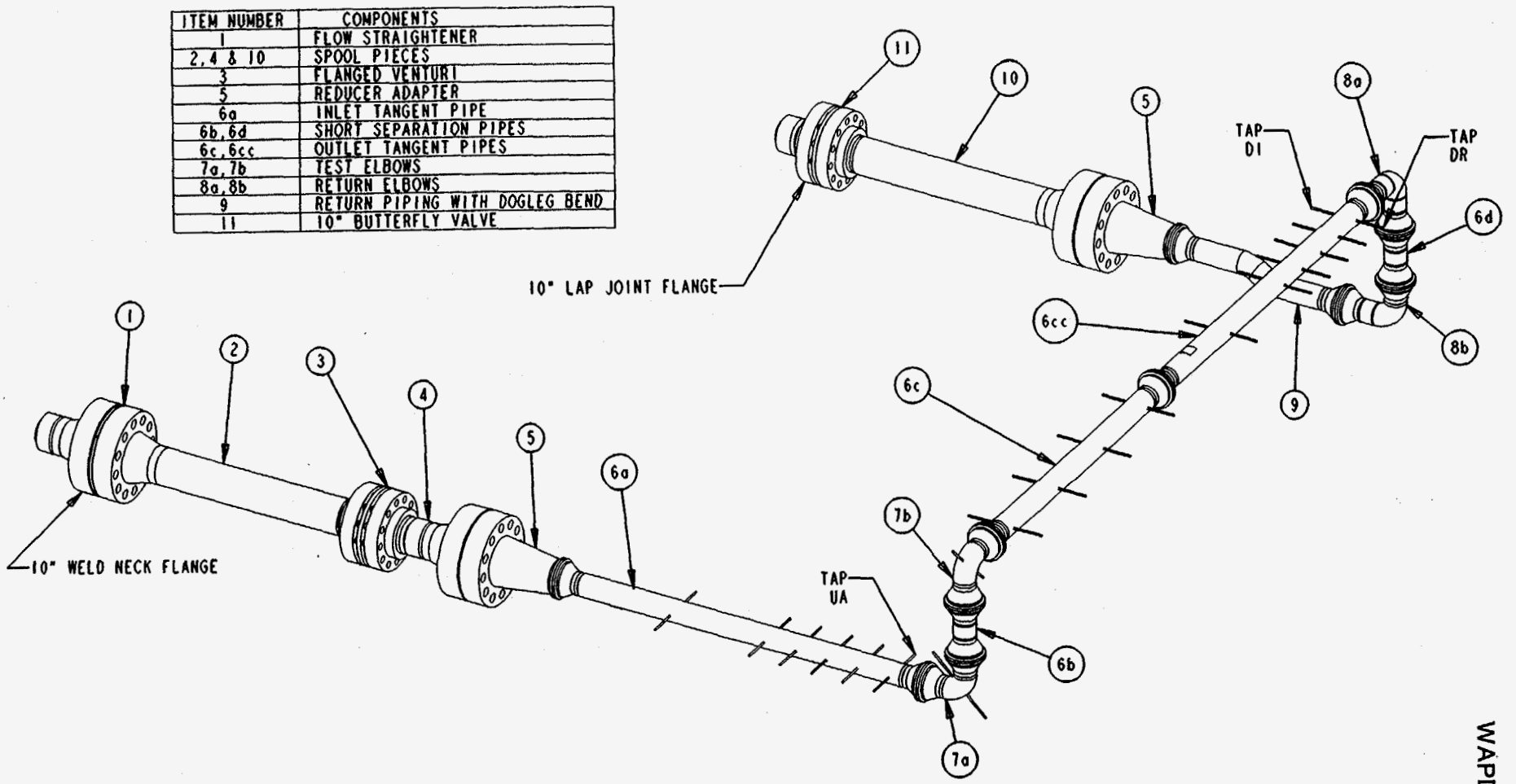

FIGURE 2.1b
Major Components for High Reynolds Number Multiple Elbow Test (With Small Separation Pipes, $L_s/D = 6.16$)

ITEM NUMBER	COMPONENT
1	FLOW STRAIGHTENER
2, 4 & 10	SPOOL PIECES (10 INCH PIPING)
3	FLANGED VENTURI
5	REDUCER ADAPTER
6a	INLET TANGENT PIPE
6bb, 6dd	LONG SEPARATION PIPES
6c, 6cc	OUTLET TANGENT PIPES
7a, 7b	TEST ELBOWS
8a, 8b	RETURN ELBOWS
9	RETURN PIPING WITH DOGLEG BEND
11	10" BUTTERFLY VALVE

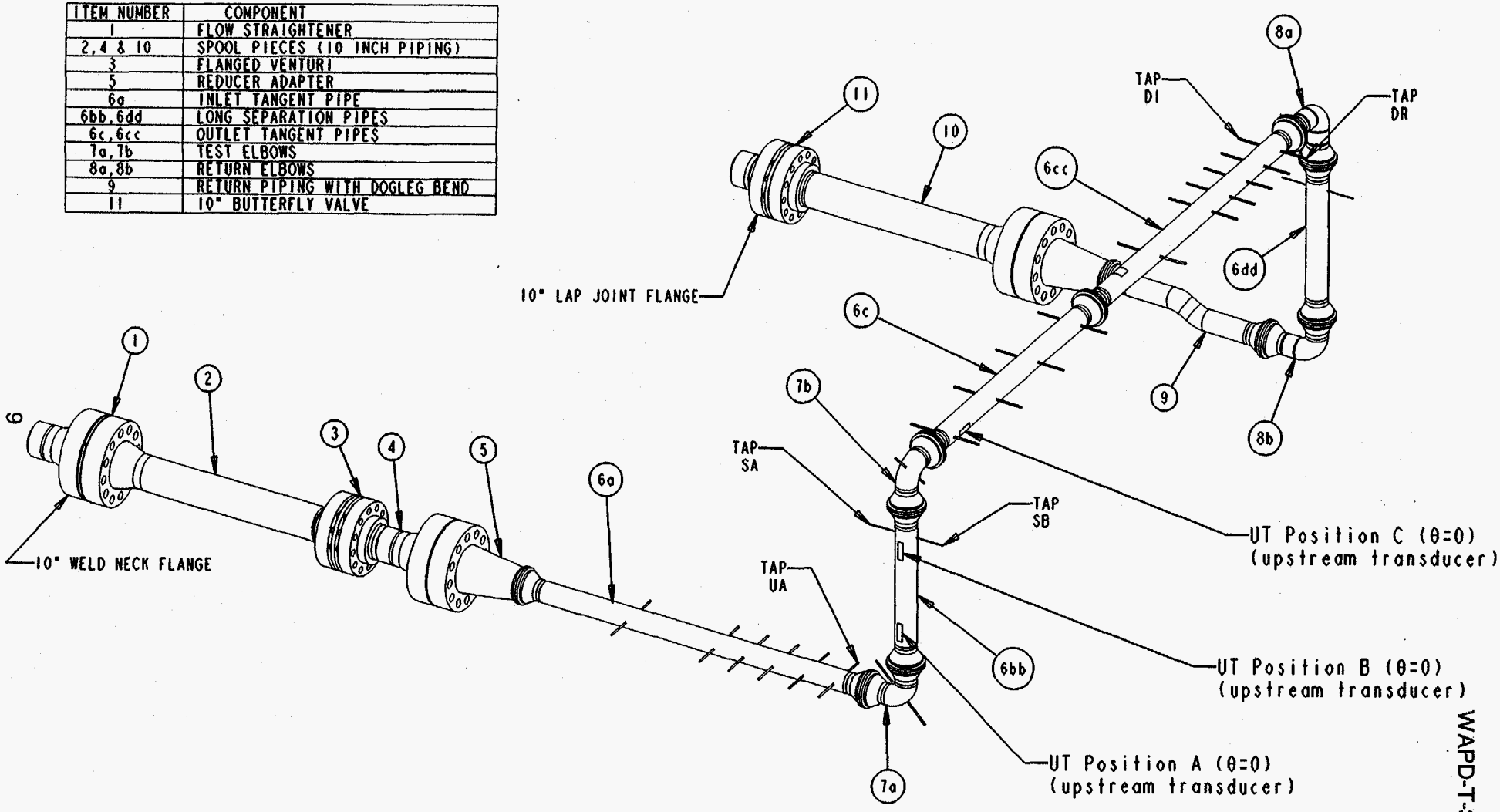

FIGURE 2.1c
Major Components for High Reynolds Number Multiple Elbow Test (With Long Separation Pipe, $L_s/D = 13.66$)

ITEM NUMBER	COMPONENT
1	FLOW STRAIGHTENER
2, 4 & 10	SPOOL PIECE
3	FLANGED VENTURI
5	REDUCER ADAPTER
6a	INLET TANGENT PIPE
6b, 6d	SHORT SEPARATION PIPES
6bb, 6dd	LONG SEPARATION PIPES
6c, 6cc	OUTLET TANGENT PIPES
7a, 7b	TEST ELBOWS
8a, 8b	RETURN ELBOWS
9	RETURN PIPING WITH DOGLEG BEND
11	BUTTERFLY VALVE

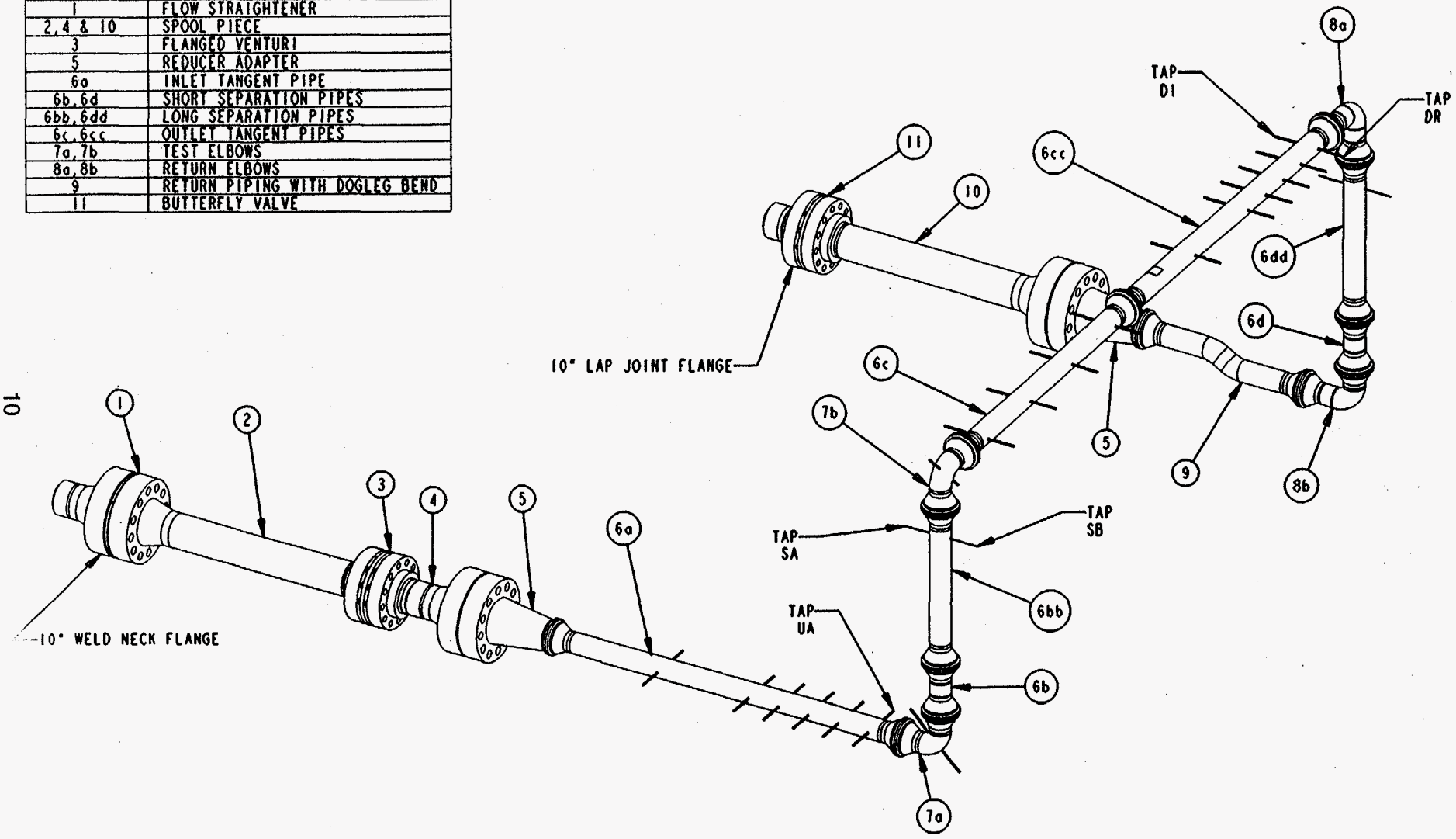

FIGURE 2.1d
Major Components for High Reynolds Number Multiple Elbow Test (With Both Separation Pipes, $L_s/D = 16.66$)

3.0 DIFFERENTIAL PRESSURE MEASUREMENTS

Differential pressures were measured between upstream pressure tap "UA" and downstream taps "DI" and "DR." These positions are shown by Figure 2.1. The downstream positions are equally spaced from the upstream tap position but are diametrically opposite sides of the pipe. These taps were confirmed to provide good pressure measurements based on the earlier single elbow test program (Reference (b)).

Differential pressure (DP) cells with the following ranges were used.

-50 to +25 in. H_2O
-50 to +200 in. H_2O
-50 to +950 in. H_2O
-50 to +1500 in. H_2O

The same upstream reference pressure tap fed into the appropriate side of each of these DP cells.

The total distance from UA to downstream taps DI and DR for the four separation distances tested was:

Separation Distance (L_S/D)	Relative Tap Position* (L/D)
3.16	48.388
6.16	51.388
13.66	58.888
16.66	61.888

* Distance does not include elbow arc lengths

4.0 SURFACE ROUGHNESS

The smooth surface for the test elbows and inlet/outlet tangent piping was fabricated by Fin-Tech, Inc. of Houston, Texas. The surface measured a roughness average (Ra) of about 15 microinches which was produced by using a flapper wheel honing process developed by Fin-Tech for mechanical polishing.

The absolute roughness, ϵ, is based on the averaged height of the surface asperities. The ratio of ϵ to the pipe inside diameter, D, is called the relative roughness, RR. Assuming the surface roughness shape is approximated by a sine wave of amplitude, A, and using the definition of Ra that it is the arithmetic mean of the absolute departures of the roughness profile, Z(x), from the mean line over a measurement length, L,

$$Ra \equiv \frac{1}{L}\int_o^L |Z(x)|\,dx$$

gives with Z(x) = A·sin x and L = 2π that

$$Ra = \frac{1}{2\pi}\int_{o}^{2\pi} |A\cdot\sin x|\,dx = \frac{2A}{\pi}$$

and since the absolute roughness is based on the overall height which is twice the amplitude then

$$\epsilon = \pi\cdot Ra$$

The magnitude of Ra is an output of various surface roughness measuring devices since it is the most used international parameter of roughness.

Pipe walls are considered to either be hydraulically smooth or rough, with the roughness being either uniform or nonuniform. These two types of roughness differ according to the shape of the surface protuberances and the spacing between them. Generally, commercial pipes are considered to have nonuniform roughness. For uniform roughness pipes, the friction factor, f, of the fluid with the wall can increase with increasing Reynolds number. This is due to the thickness of the laminar sublayer on the piping surface becoming less than the height of the surface asperities. The asperities enhance the formation of vortices and a general increase in pressure loss due to the increased form drag which develops. At lower velocities, where the asperities are contained within the viscous sublayer, the roughness has small effect on the flow behavior and the friction factor follows the characteristics of smooth tubes relative to its Reynolds number dependence. The relationship (Reference (i)) predicts the laminar sublayer thickness

$$\delta = 4\sqrt{8}\left[D/\left(Re\sqrt{f}\right)\right]$$

where: δ = laminar sublayer thickness
D = pipe inside diameter
Re = Reynolds number
f = friction factor

For the 15 microinches (Ra) roughness, the Reynolds number at which the laminar sublayer would be approaching the full height of the surface asperities would be about 22×10^6. At higher Reynolds numbers, the roughness protrudes above the laminar sublayer and thus a change in the friction factor versus Reynolds number characteristic would be expected due to the additional form drag developed by the higher velocity flow passing over the protrusions. This change can be noted to occur in the measured friction factor (described in Section 6.0) at about this predicted Reynolds number in the form of a flattening of the friction factor curve above 24×10^6 Reynolds number. Once the surface roughness protrudes outside the laminar sublayer, the irrecoverable pressure loss becomes dominated by the profile drag of the asperities which has a low Reynolds number sensitivity compared to the viscous sublayer influence which is strongly Reynolds number dependent.

5.0 METHODS USED TO ESTIMATE IRRECOVERABLE PRESSURE LOSS COEFFICIENT UNCERTAINTY

The irrecoverable loss coefficient (K) was calculated from the relationship:

$$K = \Delta P/(\rho V^2/2g_c) - f(L/D)$$

where:

ΔP = Pressure loss measurement between a reference pressure tap just upstream of the elbow and a tap position sufficiently far downstream from the elbow to allow flow recovery

ρ = Fluid density

V = Fluid velocity

L = Distance between pressure measurements

D = Inside pipe diameter

f = Friction factor

The uncertainties associated with this equation are provided by the following relationships.

$$\{ [\Delta P/(\rho V^2/2g_c)] \pm UC1\} - \{(f(L/D)] \pm UC2\} = K \pm UC3$$

where:

$$UC1 = UC1M + UC1B$$

with

$UC1M$ = Total measurement uncertainty. The test instrumentation was designed to maintain this value to less than 1.0%. The venturi measurement for flow rate had less than ± 0.25% uncertainty based on calibration. Multiple range differential pressure cells were used in parallel to minimize pressure loss measurement uncertainties.

$UC1B$ = Total pressure loss measurement bias attributed to burrs/surface imperfections, local surface roughness effects and flow non-recovery (based on measurements to diametrically opposite sides of the downstream tangent pipe for the reference tap positions). The taps were verified to be free of burrs by touch and visual examination. Fiber optics were used to inspect remote positions.

and

$UC2$ = Combined uncertainty due to friction factor and dimensional uncertainties.

$$UC2 = \pm\sqrt{\left(\frac{\Delta L}{L}\right)^2 + \left(\frac{\Delta D}{D}\right)^2 + \left(\frac{\Delta f}{f}\right)^2}$$

The UC1 and UC2 uncertainties are assumed independent and cause $(\Delta K/K)_1$ and $(\Delta K/K)_2$ respective uncertainties on the nominal K value. The total test uncertainty on K, defined as UC3, is then:

$$UC3 = \pm\sqrt{\left(\frac{\Delta K}{K}\right)_1^2 + \left(\frac{\Delta K}{K}\right)_2^2}$$

Using this approach resulted in a maximum uncertainty range of ±20%.

This methodology for assessing the total uncertainty is consistent with those reported to provide at least a 2σ level of confidence on the uncertainty.

6.0 FRICTION FACTORS BASED ON MEASURED PRESSURE GRADIENTS

Figure 6.1 shows typical examples of Reference (a) data at Reynolds numbers of 1, 18 and 36 x 10^6. The pressure ratio $[\Delta P/(\rho V^2/2)]$ is plotted as a function of axial position in the test piping. The dynamic head $(\rho V^2/2)$ is based on the average velocity in the test piping. Reynolds numbers from 0.5 x 10^6 to about 40 x 10^6 were tested. Data was recorded every five seconds for a total of twenty-one measurements at each position. All measurements are individually plotted at each tap position shown on the figures, thus each position has a clustering of about 42 separate measurements from the two taps (opposite sides of the pipe) which were located at each axial position. As can be noted, reasonably consistent data groupings were achieved spatially throughout the test piping.

Because of the well established turbulent flow field in the inlet tangent piping (confirmation measurements described in Reference (b)), its pressure gradient was used to define the friction factor where:

$$f = \Delta P/[(\rho V^2/2)(L/D)]$$

the friction factor at a particular axial position is then the slope of the curve at that position since the tap positions have been plotted with respect to distance in piping diameters (i.e., L/D's). All taps were used in a linear regression curve fit to establish the gradient. The straight line curve fit resulting from the linear regression analysis are shown on each of the figures and, as can be noted, good agreement was consistently achieved.

The friction factors derived from each of the upstream pressure gradients are shown by Figure 6.2. The smooth roughness is within 5% of that given by the Colebrook relationship (Reference (j)). Similar to the trend found in Princeton friction factor measurements (Reference (h)), the data tends to run higher than that derived from the earlier databases. For the almost perfectly smooth Princeton piping, the differences ranged from about 3% at Re = 10^6 to about 7% at Re = 35 x 10^6. Both the Princeton and Reference (b) measurements are reasonably close to the uncertainty bands of the earlier data (±5% as reported in Reference (j)).

FIGURE 6.1

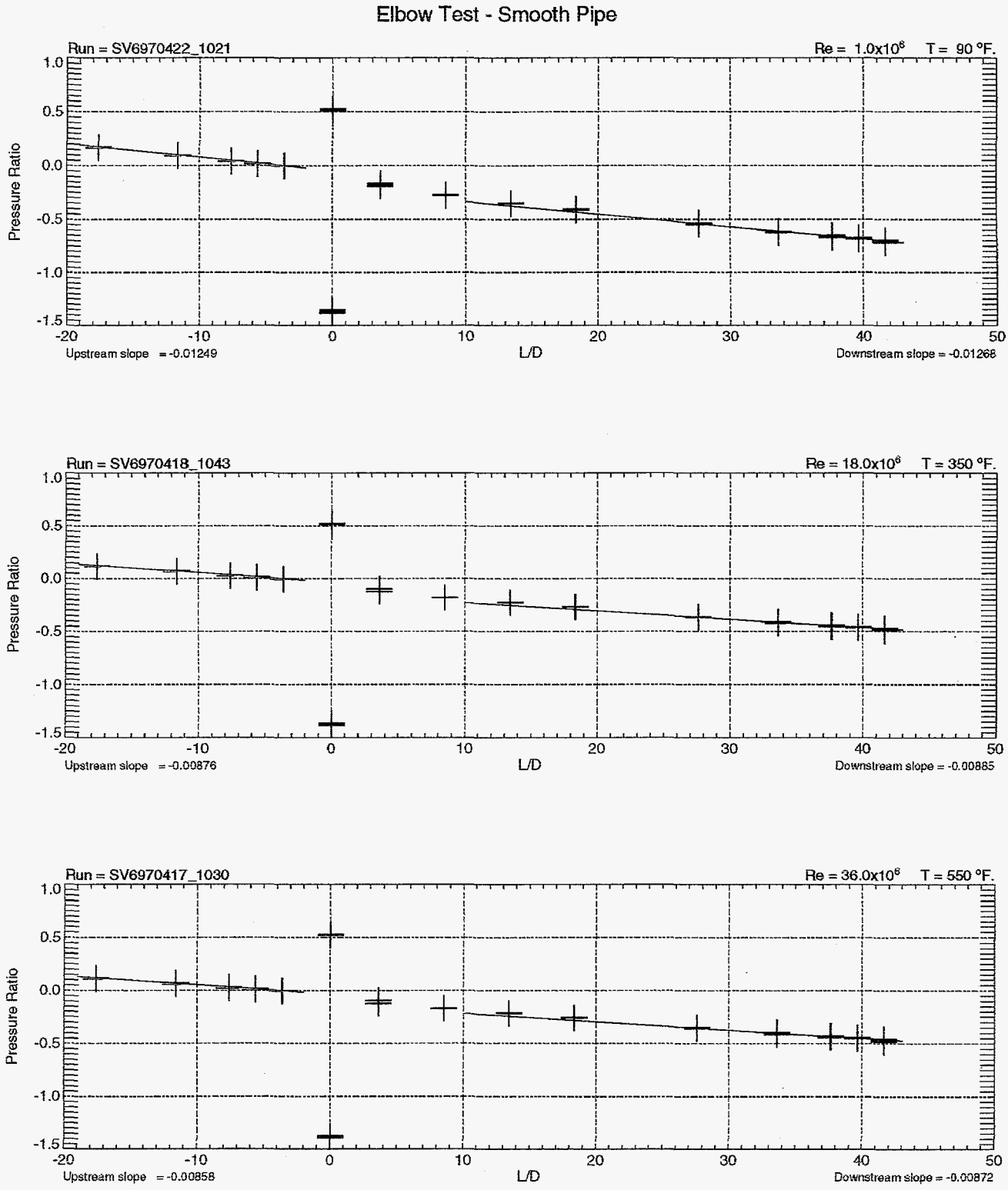
Elbow Test - Smooth Pipe
Run = SV6970422_1021
Re = 1.0x10^6 T = 90 °F.
Pressure Ratio
1.0
0.5
0.0
-0.5
-1.0
-1.5
-20
-10
0
10
20
30
40
50
L/D
Upstream slope = -0.01249
Downstream slope = -0.01268
Run = SV6970418_1043
Re = 18.0x10^6 T = 350 °F.
Pressure Ratio
Upstream slope = -0.00876
Downstream slope = -0.00885
L/D
Run = SV6970417_1030
Re = 36.0x10^6 T = 550 °F.
Pressure Ratio
Upstream slope = -0.00858
Downstream slope = -0.00872
L/D

FIGURE 6.2

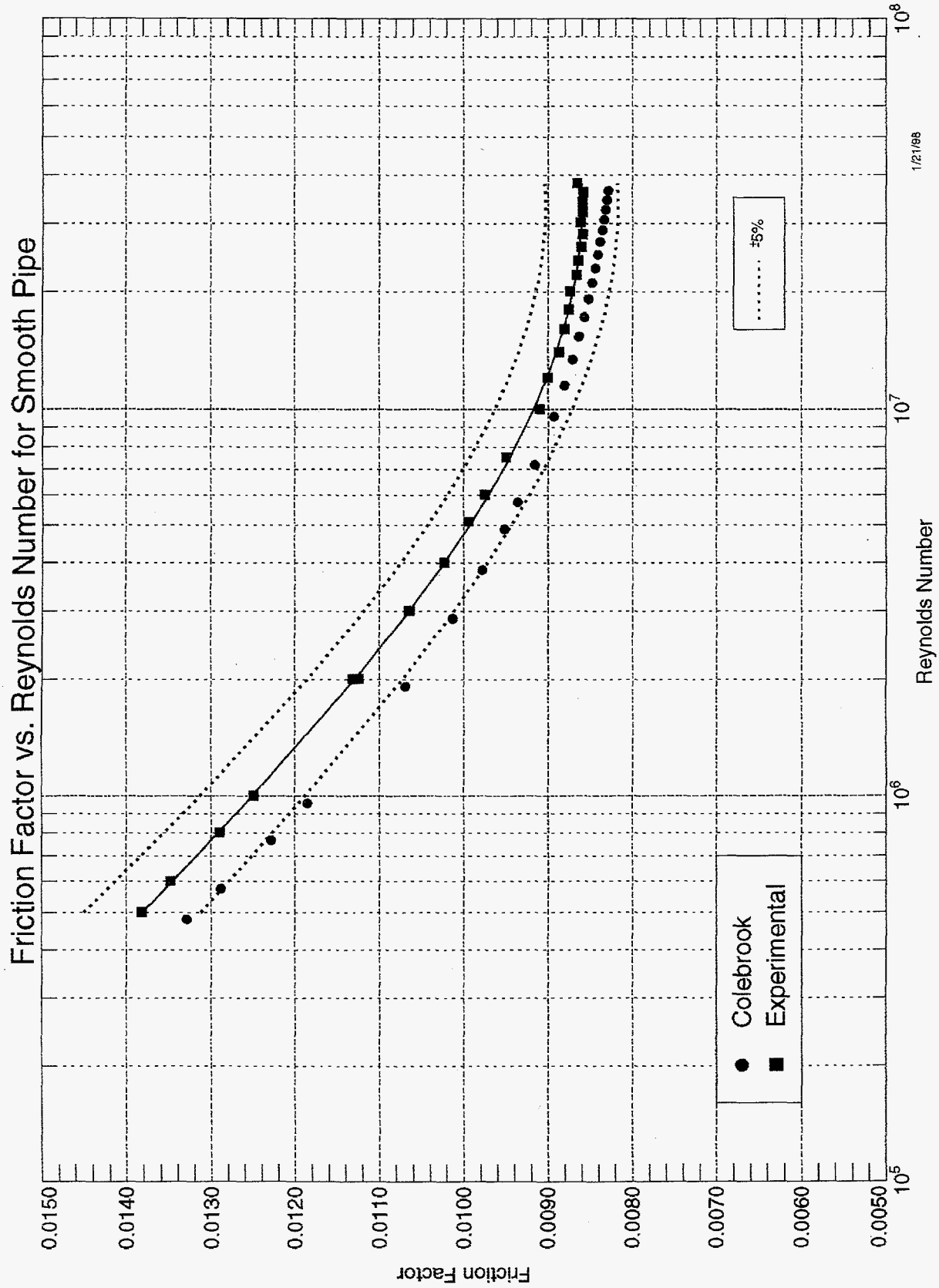

FIGURE 6.2

7.0 ELBOW IRRECOVERABLE PRESSURE LOSS COEFFICIENTS AS FUNCTION OF REYNOLDS NUMBER

To determine the test elbow irrecoverable loss coefficient over a wide Reynolds number range, the loop flow and temperature were varied while the pressure loss from upstream of the elbow to a position near the exit of the test outlet piping was measured. A Reynolds number range from 0.6×10^6 to 37.0×10^6 was covered. The loss coefficient was calculated by the relationship defined in Section 6

$$K = \Delta P/(\rho V^2/2g_c) - f(L/D) \qquad \text{(Eq. 7.1)}$$

This total loss coefficient for the two test elbows was divided by two to give an average irrecoverable loss coefficient (K).

The testing was conducted in three segments termed "sweeps" which covered the following Reynolds number ranges.

Sweep	Loop Temperature (°F)	Reynolds Number Range
1	550	37×10^6 to 10×10^6
2	350	10×10^6 to 2.5×10^6
3	200	2.5×10^6 to 0.5×10^6

The loop flow was programmed to automatically decay by slowly decreasing the pump voltage frequency from the motor-generator. Figure 7.1 shows the rate of flow decay for Sweep 1 which typifies those for the other two sweeps. Data was recorded every five seconds by the data acquisition system. For the full test (Sweeps 1, 2, and 3) about 3800 irrecoverable loss coefficient measurements were made over the 0.6 to 37.0×10^6 Reynolds number range. Figures 7.2 to 7.5 show the measurements for each respective separation distance using UA as the upstream tap and DI (red color) and DR (green color) as the downstream taps. The measured friction factors for the smooth piping described in Section 6 were used for the loss coefficient prediction using Equation 7.1.

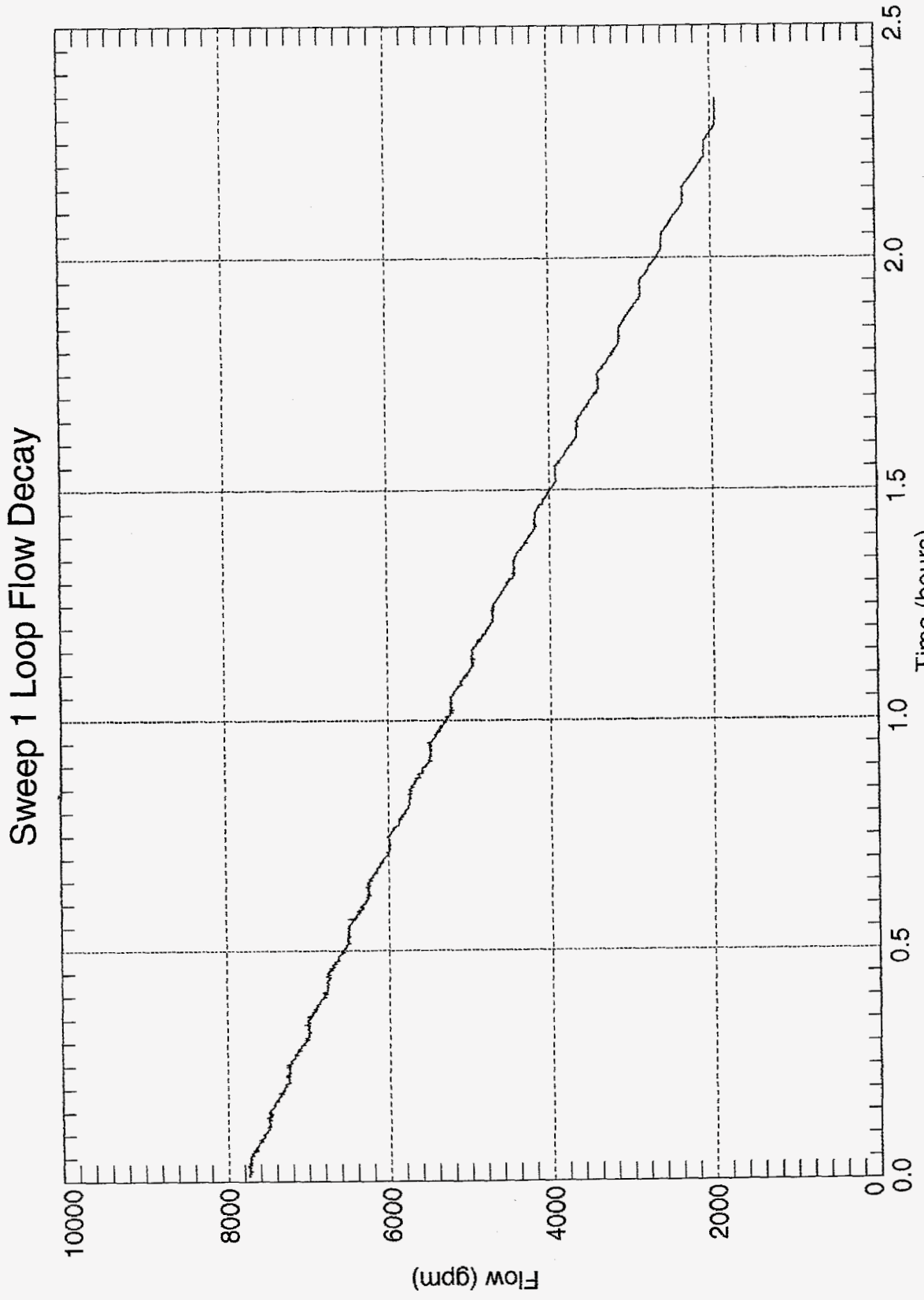
Sweep 1 Loop Flow Decay
Flow (gpm)
10000
8000
6000
4000
2000
0
0.0
0.5
1.0
1.5
2.0
2.5
Time (hours)

FIGURE 7.1

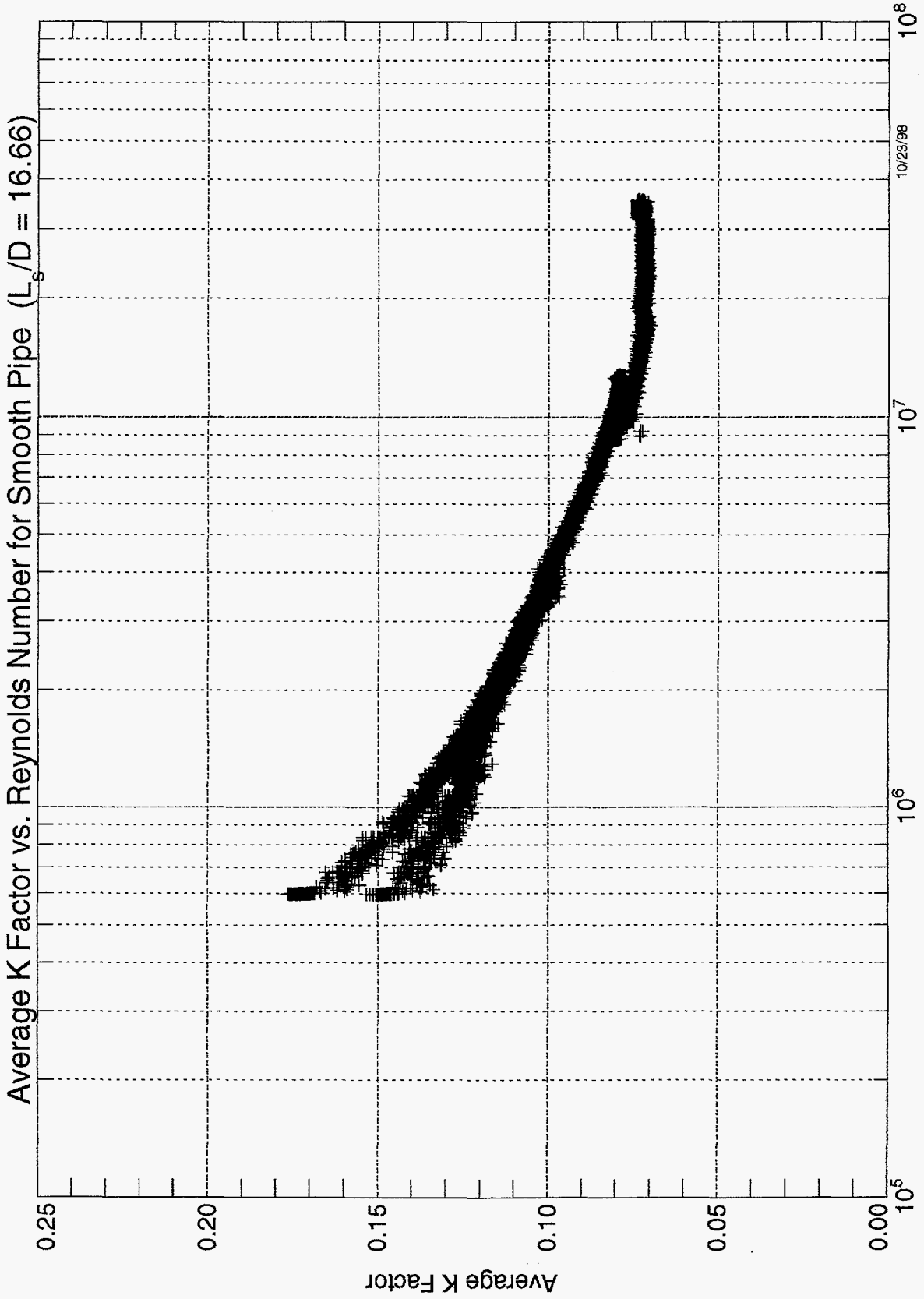
Average K Factor vs. Reynolds Number for Smooth Pipe (L_s/D = 16.66)
Average K Factor
0.25
0.20
0.15
0.10
0.05
0.00
10^5
10^6
10^7
10^8
Reynolds Number
10/23/98

FIGURE 7.2

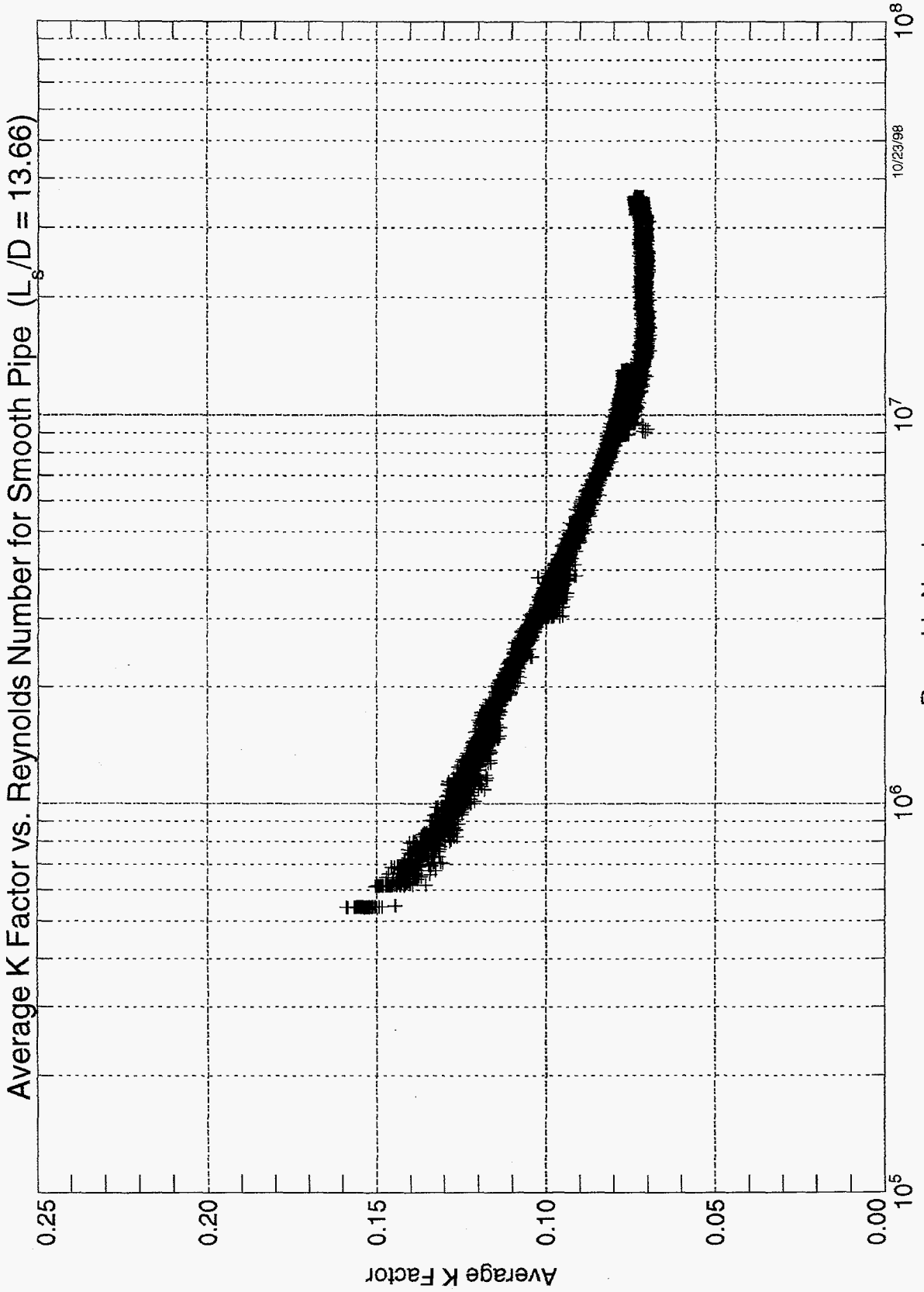
Average K Factor vs. Reynolds Number for Smooth Pipe (L_s/D = 13.66)
Average K Factor
0.25
0.20
0.15
0.10
0.05
0.00
10^5
10^6
10^7
10^8
Reynolds Number
10/23/98

FIGURE 7.3

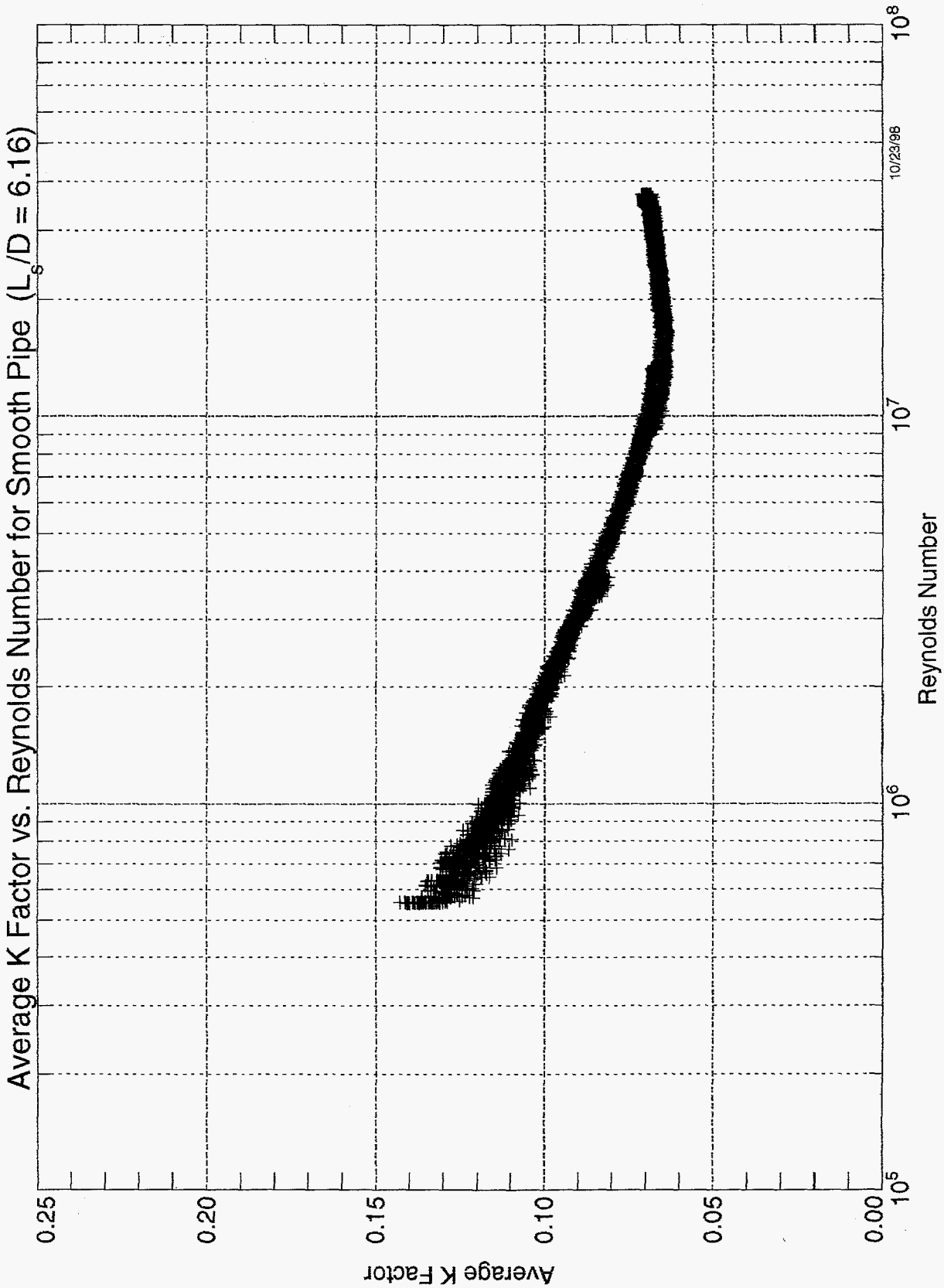
Average K Factor vs. Reynolds Number for Smooth Pipe (L_s/D = 6.16)
10/23/98
Average K Factor
0.25
0.20
0.15
0.10
0.05
0.00
10^5
10^6
10^7
10^8
Reynolds Number

FIGURE 7.4

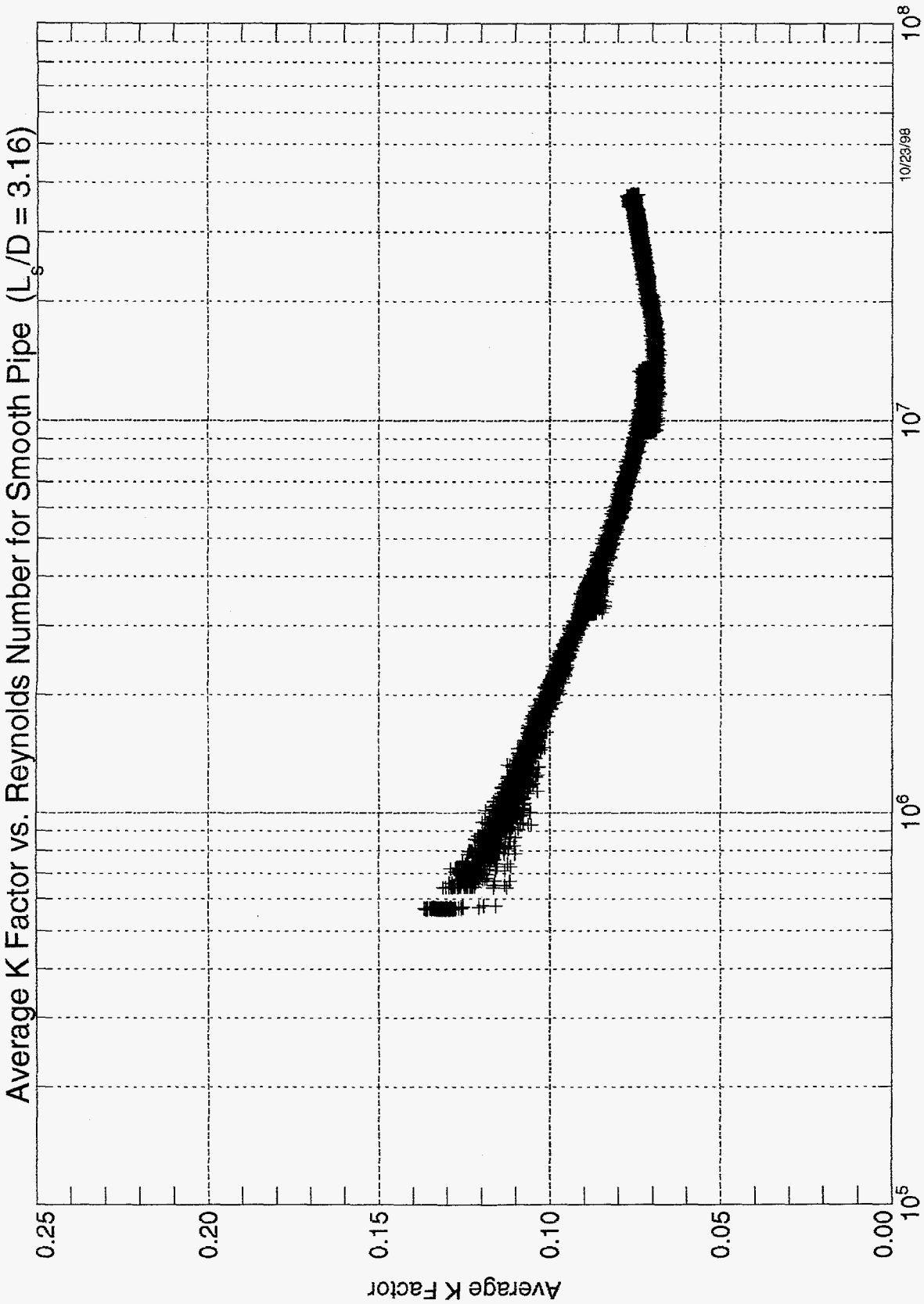
Average K Factor vs. Reynolds Number for Smooth Pipe (L$_s$/D = 3.16)
Average K Factor
0.25
0.20
0.15
0.10
0.05
0.00
10^5
10^6
10^7
10^8
Reynolds Number
10/23/98

FIGURE 7.5

8.0 ULTRASONIC FLOWMETER MEASUREMENTS

Ultrasonic flowmeter measurements were recorded at positions noted on Figure 2.1c as A and B after the first test elbow and position C after the second test elbow. Relative to the outlet of each respective elbow these axial positions in piping diameters are:

Position (see Figure 2.1c)	Axial Position (L/D's)
A	4.4
B	9.0
C	5.3

A Controlotron Model 1010 ultrasonic flowmeter was used for the measurements. An upstream and a downstream transducer (located on opposite sides of the pipe) were used to transmit acoustic waves across the pipe fluid toward each other. A direct travel-time configuration was used to measure the time difference between the upstream and downstream signals. This method utilizes the fact that the travel distance for the acoustic wave is known along with the acoustic velocity for the fluid condition. The velocity component of the flow field in the path direction then determines the time to travel the path length (i.e., travel time equals distance divided by velocity in the path direction). When the signal is moving in the flow direction, the effective velocity is increased and when the signal is against the flow direction the effective velocity is decreased. The ultrasonic flowmeter has built-in algorithms that convert the shift in travel time (between the acoustic waves moving with and against the flowstream) into an average flowrate. The meter assumes a flow profile for fully developed turbulent flow in order to convert the travel time shift into average volumetric flowrate. As long as the flow profile is similar to the assumed profile, good accuracy in predicting the volumetric flowrates has been achieved. However, if cross-flow effects are present such as those due to swirl and flow maldistribution, inaccuracies in the measurements develop. The objective of the testing was to provide data so that computational fluid dynamics (CFD) predictions of the flow field could be used to simulate the same travel time conditions as experienced by the ultrasonic flowmeter measurements. A comparison of the relative error between the CFD simulation and meter measurements could then be interpreted as a confirmation of the CFD predicted flow profile. This approach had been suggested by Reference (k) but ultrasonic flowmeter measurements were not available to test the feasibility of the method.

For eight equally spaced circumferential positions around the pipe (45° intervals) ultrasonic flowmeter measurements were recorded. The zero angular position was taken to be the outside pipe wall for the plane orthogonal to the elbow radius of curvature with increasing angles being in the counter-clockwise direction when viewed toward the downstream direction (see Figure 2.1c). The velocity measurement at each angular position is divided by the average of all eight velocity measurements at the particular axial position. The ratio has been termed the relative velocity ratio. Figures 8.1, 8.2, and 8.3 show the variation in the

relative velocity ratio with angular orientation around the pipe at axial positions A, B, and C, respectively. Data is provided for Reynolds numbers of 1 x 10^6 and 3 x 10^6. As can be noted, positions A and B after the first elbow depict a negative variation over the first 180° of measurements and a positive variation over the second 180° of measurements. This effect is representative of the counter rotating vortices that develop downstream of a piping elbow. The measured data has been superimposed on the CFD results predicted by Reference (k) on Figure 8.4 and as can be noted excellent agreement was found. The Loop 6 data corresponds to $\phi = 65.4°$ (slope of sonic wave diametrically crossing the pipe) and a separation distance of 4.4 piping diameters which are close to the prediction conditions of $\phi = 60°$ and 5.0 piping diameters separation. The position B data shows that the vortices still exist but are of less intensity after the additional 4.6 diameter travel downstream. The measurements after the second elbow do not exhibit the same characteristics. This position suggests that only a single vortex exists that is eccentrically located relative to the pipe centerline. Reference (a) studied single vortices that were symmetric and concluded that no angular orientation would be measured. Eccentricity would asymmetrically increase transverse velocities to the sonic wave path length which would result in an increased dependence in angular dependence as measured in the test.

One postulated mechanism for the difference between positions A and B relative to C is that one of the two vortices from the first elbow is destroyed by the second elbow. The destroyed vortex would be the one that impacts the second elbow in its high pressure outer surface position which would tend to split this vortex into two streams that are seeking to flow in opposite directions around the circumference to the low pressure inner side of the second elbow. The splitting forces could result in destruction of the impacting vortex. CFD investigations should help substantiate the controlling mechanisms that produce the Figure 8.3 measurements for position C.

The average of the eight velocity measurements, $\bar{u}_{axial}$, at each axial position has been normalized to the average velocity measured upstream of the first elbow (where it has been substantiated that a fully developed turbulent velocity profile exists), $\bar{u}_{inlet}$, to give:

Position	$\bar{u}_{axial}/\bar{u}_{inlet}$	
	Re = 1 x 10^6	Re = 3 x 10^6
A	0.925	0.917
B	0.927	0.925
C	0.963	0.955

The $\bar{u}_{axial}$ measurement has ideal measurement conditions relative to the intended application of the ultrasonic flowmeter. Thus, the variation of $\bar{u}_{axial}/\bar{u}_{inlet}$ provides an indication of the error induced by the cross flow velocity components influencing the measurements. A maximum error of 8.87% [(1.000 - 0.917) x 100%] can be noted for these particular measurements.

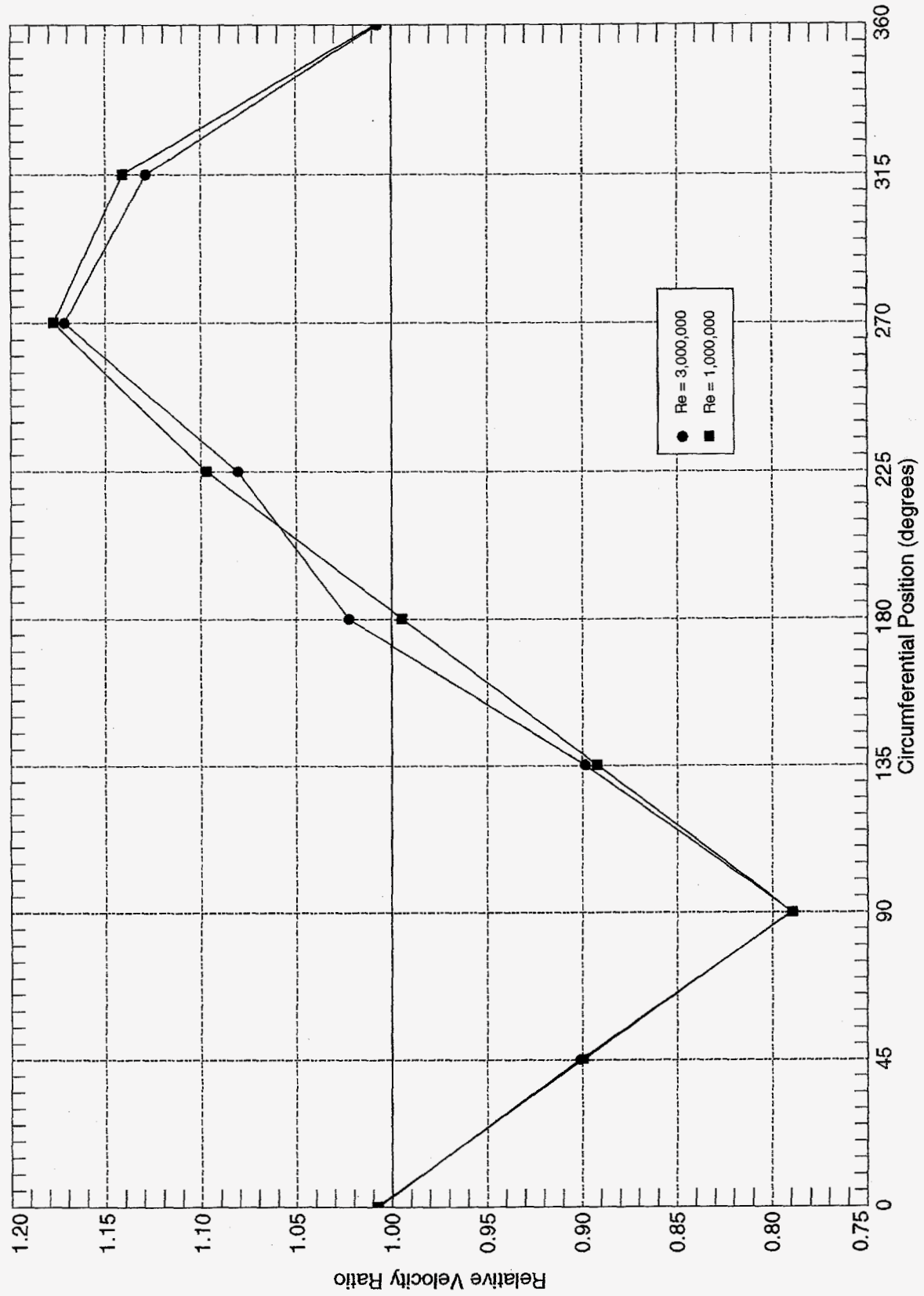

FIGURE 8.1
Ultrasonic Flowmeter Data
Axial Position A

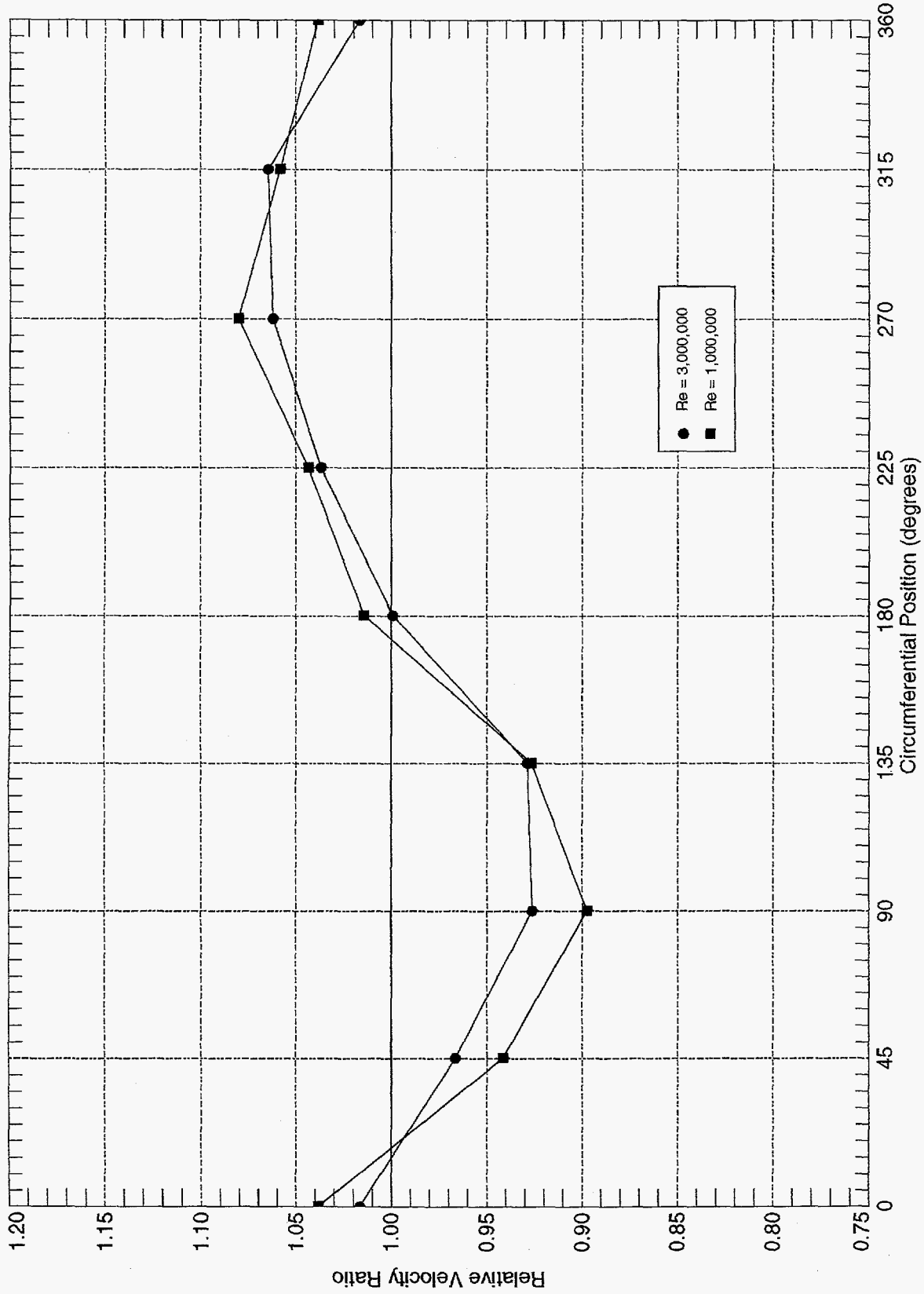

FIGURE 8.2
Ultrasnoic Flowmeter Data
Axial Position B

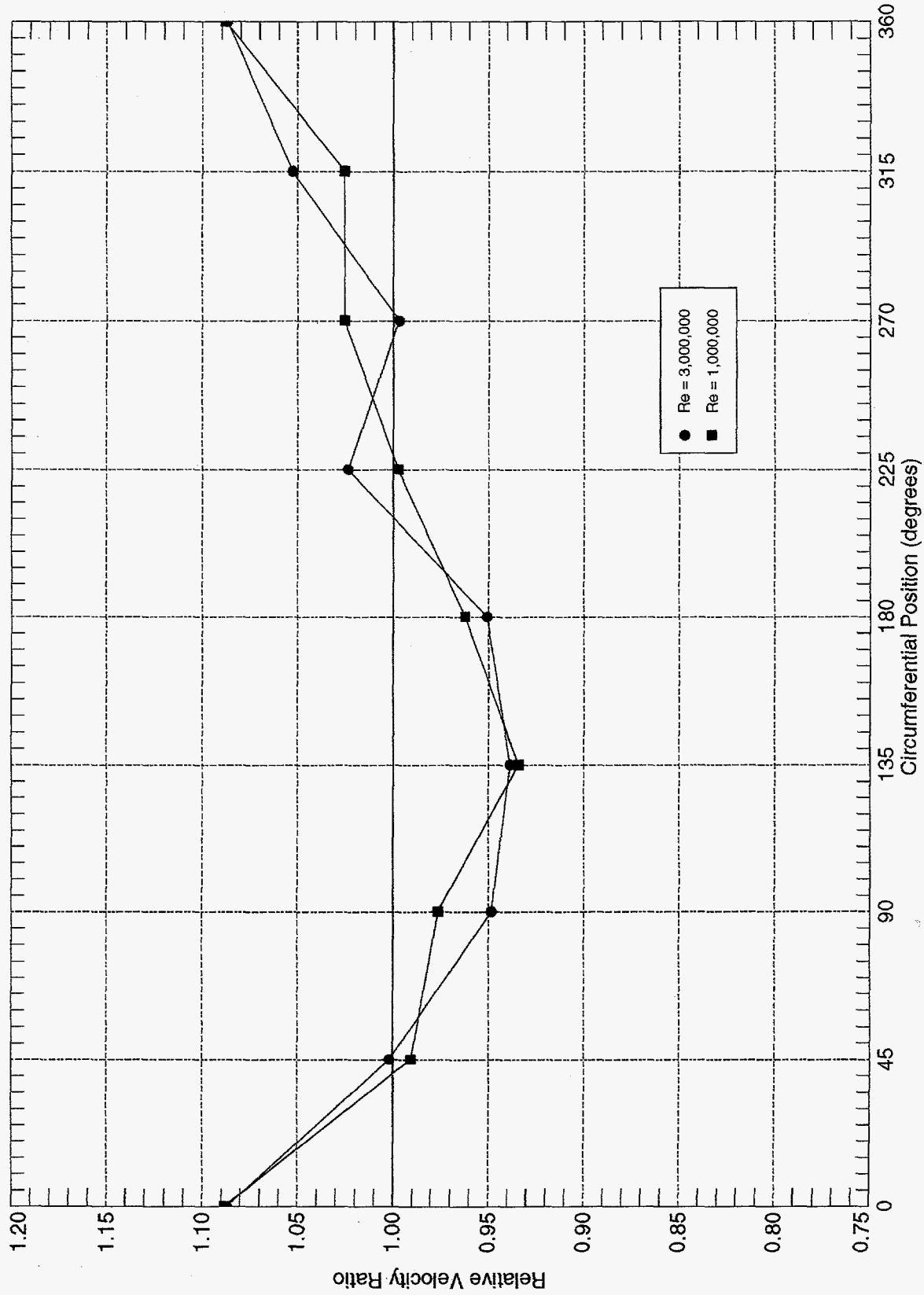

FIGURE 8.3
Ultrasonic Flowmeter Data
Axial Position C

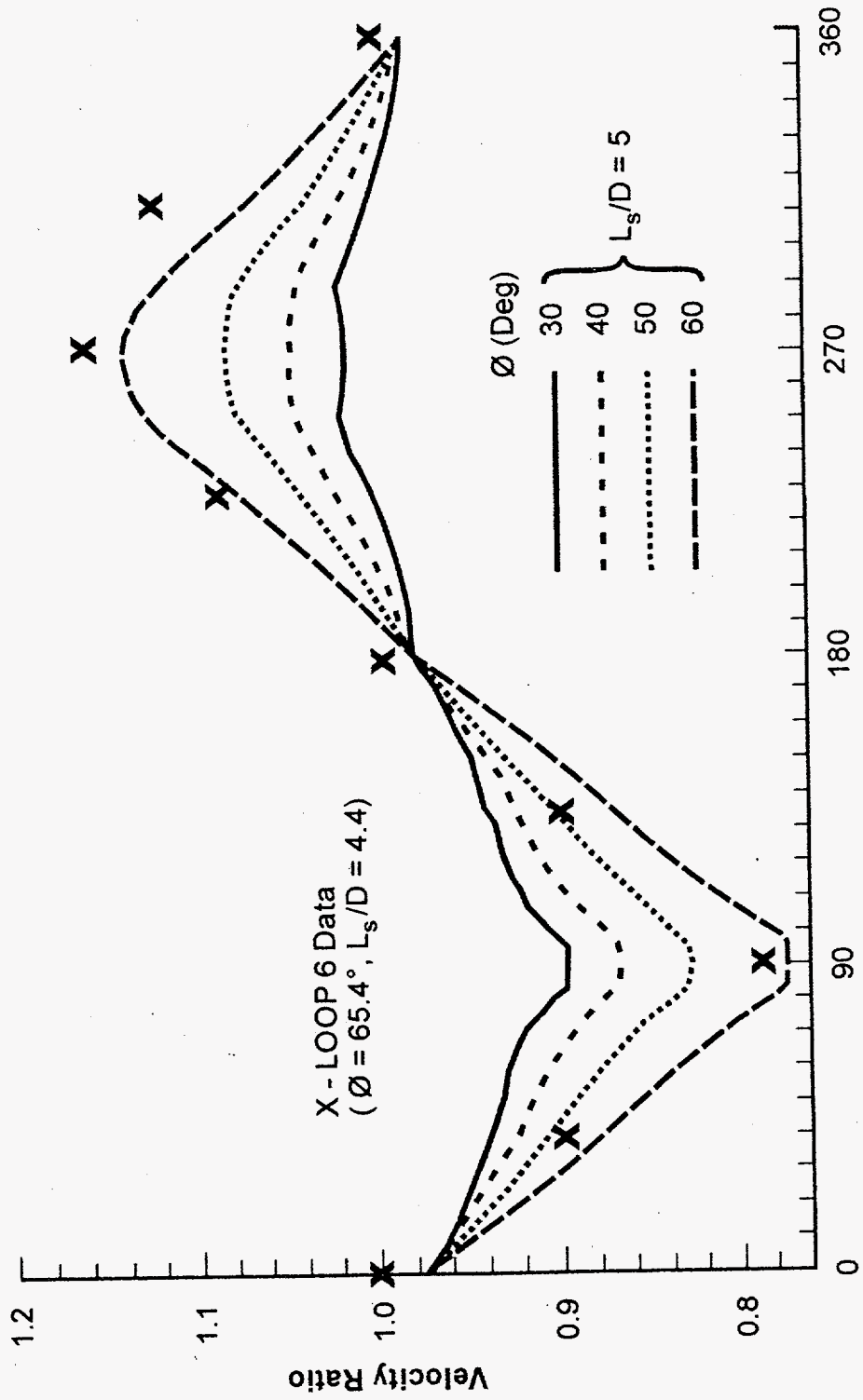

FIGURE 8.4
Comparison of Loop 6 Ultrasonic Velocity Measurements to NIST Analytical Predictions

9.0 SUMMARY AND CONCLUSIONS

The results of the ultrasonic flowmeter testing described in Section 8.0 look encouraging relative to indicating vortex flow patterns in the flow field. Good agreement of the measurements to computational fluid dynamics (CFD) predictions for the same modeling conditions as tested will help validate that the CFD predicted flow fields are accurate. The Section 8.0 data was shown to agree well to published CFD results (Reference (k)) for flow after a single elbow.

Figure 9.1 shows a summary of the irrecoverable loss coefficients for a single elbow with a 15 microinch surface finish (Ra) that were measured in the Reference (b) testing. A current design correlation (based on Reference (e)) is shown for comparison purposes. As can be noted, the design curve is about 200% conservative at high Reynolds numbers (i.e., $Re > 24 \times 10^6$).

Figure 9.2 shows a summary of the average irrecoverable pressure loss coefficient measurements for all separation distances tested. The separate pressure tap measurements shown by Figures 7.2, 7.3, 7.4, and 7.5 were averaged for each separation distance. The 16.66 diameter separation distance data was found to be approximately the same as that for the single elbow reported in Reference (b) and shown by Figure 9.1. Thus, it was concluded that the 16.66 diameter separation resulted in minimal elbow interaction effects. However, as the spacing was decreased, interaction effects between the elbows were found to occur. To quantify this interaction, the average irrecoverable loss coefficient for the two elbows was divided by the irrecoverable loss coefficient for a single elbow to give a ratio factor:

$$R = \text{average k/single elbow k}$$

This ratio was plotted as a function of separation distance from various Reynolds numbers in Figure 9.3. A ratio less than 1.0 indicates that the net irrecoverable pressure loss is less than that for two separate elbows acting independently. A ratio of 1.0 is often assumed by designers who are trying to conservatively envelope the consequences of elbow interaction effects.

As can be seen on Figure 9.3, at lower Reynolds numbers (i.e., less than 1×10^6) the ratio monotonically decreases with decreasing separation distance. Also, low sensitivity to Reynolds number can be seen by comparing the respective curves for a 0.7×10^6 and 1.0×10^6 Reynolds number. This helps explain trends found in earlier low Reynolds number studies such as Reference (l) at $0.2 \times 10^6 < Re < 1.0 \times 10^6$ and in Reference (c) at $0.3 \times 10^5 < Re < 1.0 \times 10^6$. These tests were at too low a Reynolds number to enable the Figure 9.3 interaction effects to be detected and thus no Reynolds number corrections were recommended. Figure 9.3 shows that this is incorrect for higher Reynolds numbers. In fact, in the 5 to 36 $\times 10^6$ range, the data shows that as the separation distance is decreased to less than about six piping diameters, increases in the ratio factor can occur. This indicates that the net irrecoverable pressure loss starts to approach, and even somewhat surpass (for above 15×10^6 Reynolds number and approaching zero separation distances) the irrecoverable pressure loss for two separate elbows that are independent of each other (i.e., Reference (b) single elbow condition). Figure 9.4 shows the earlier separation distance predictions of References (l) and (c) superimposed on Figure 9.3 to demonstrate the need to consider the high Reynolds number influence in estimating piping interaction effects.

Figure 9.2 shows as its upper curve typical design values for irrecoverable pressure loss of multiple elbows. This curve (based on correlations recommended by Reference (e)) assumes that neglecting elbow interaction effects is conservative and that single elbow irrecoverable pressure losses can conservatively be independently added to each other to obtain a net irrecoverable pressure loss. Comparing the test data to the design curve shows that this assumption can be as much as a factor of 200% conservative at high Reynolds numbers of about 40×10^6. The increasing values of the interaction ratio with near zero separation distance and high Reynolds number can somewhat decrease this margin but it is estimated that this would be less than a 30% influence so that at least 170% of the margin would still exist for the net irrecoverable pressure loss prediction.

In addition to providing direct piping design data for elbow irrecoverable pressure loss coefficients, another objective of the testing was to provide an accurate database for qualifying the piping pressure loss predictions from Computational Fluid Dynamics (CFD) computer codes. This requires accurate flow field characterization to minimize uncertainties in basic parameters needed for the analyses and for comparisons to the data. The data meets this objective since:

- The inlet velocity profile to the test elbow was confirmed by measurements (Reference (b)) to be that for fully developed, turbulent flow in a straight pipe. It can thus be well defined for the analytical models.

- The straight pipe friction factors used for calculating the elbow irrecoverable pressure loss coefficients are based on data measurements in the inlet tangent pipe that are very consistent over the several orders of magnitude variation in Reynolds numbers and are in good agreement with Princeton University measurements for the smooth surface finish testing and Idelchik data for rough surface finish testing (described in Section 6.0).

- Pressure loss measurements from pressure taps in the straight pipe flow region upstream of the elbow to pressure taps selected downstream at a position where the flow had regained its straight pipe flow conditions were very consistent over the several orders of magnitude variation in Reynolds number. Inconsistencies of the type associated with troublesome static wall pressure taps were not detectable.

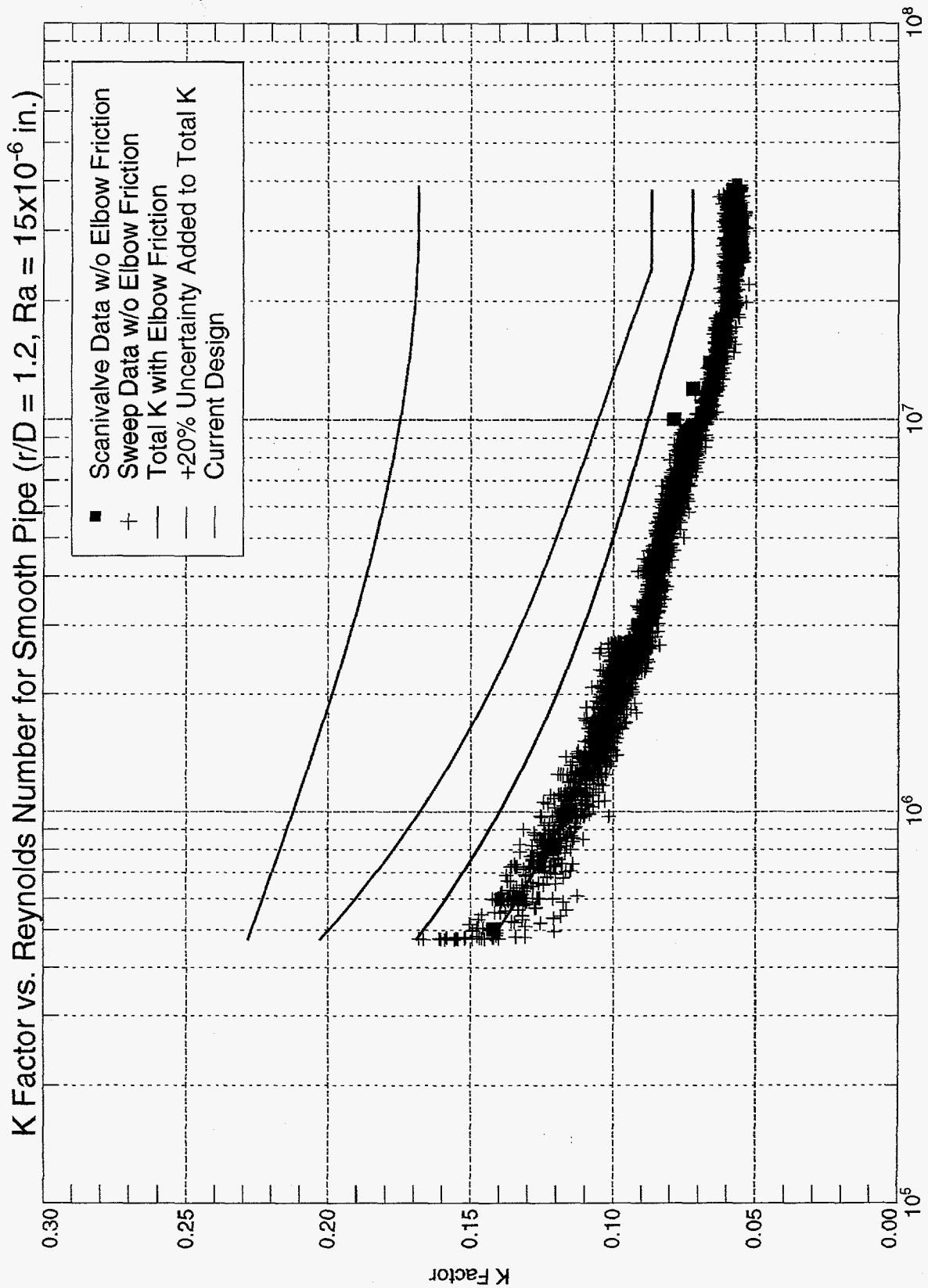
K Factor vs. Reynolds Number for Smooth Pipe (r/D = 1.2, Ra = 15x10-6 in.)
Scanivalve Data w/o Elbow Friction
Sweep Data w/o Elbow Friction
Total K with Elbow Friction
+20% Uncertainty Added to Total K
Current Design
K Factor
0.30
0.25
0.20
0.15
0.10
0.05
0.00
10^5
10^6
10^7
10^8
Reynolds Number
SV6970206_0000.1
7/29/98

FIGURE 9.1

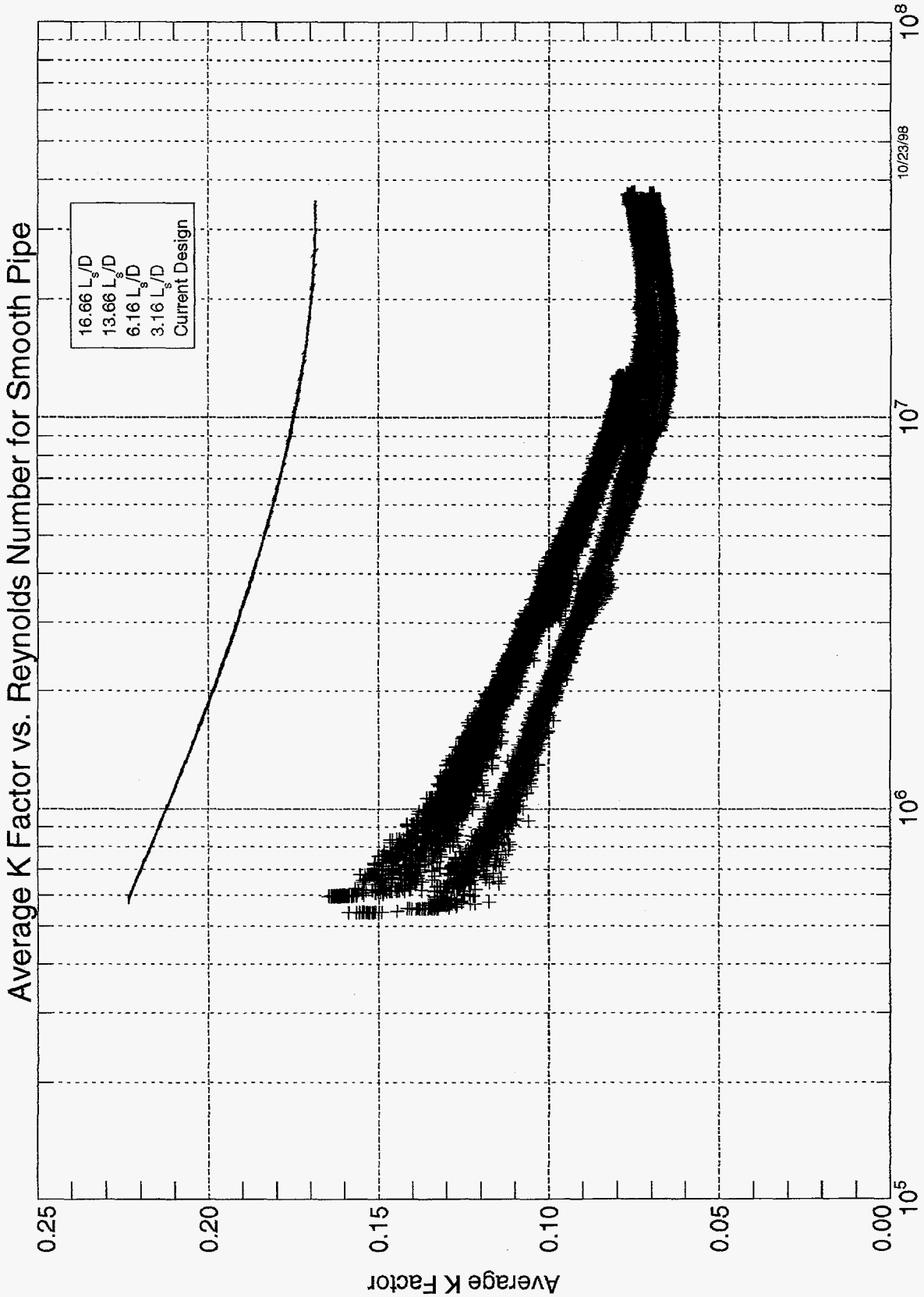
Average K Factor vs. Reynolds Number for Smooth Pipe
16.66 L_s/D
13.66 L_s/D
6.16 L_s/D
3.16 L_s/D
Current Design
10/23/98
Average K Factor
0.25
0.20
0.15
0.10
0.05
0.00
10^5
10^6
10^7
10^8
Reynolds Number

FIGURE 9.2

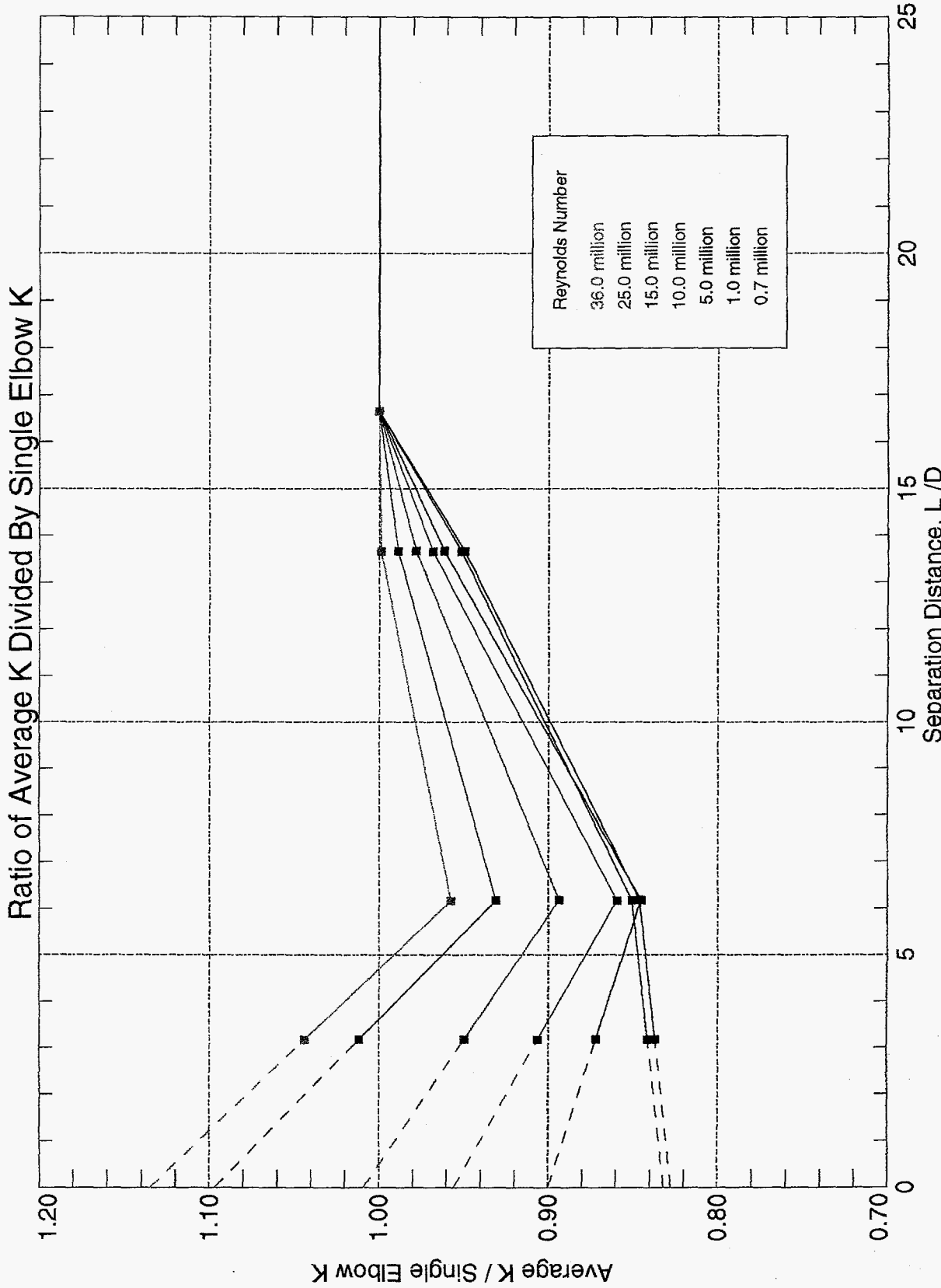
Ratio of Average K Divided By Single Elbow K
Average K / Single Elbow K
1.20
1.10
1.00
0.90
0.80
0.70
0
5
10
15
20
25
Separation Distance, L_s/D
Reynolds Number
36.0 million
25.0 million
15.0 million
10.0 million
5.0 million
1.0 million
0.7 million

FIGURE 9.3

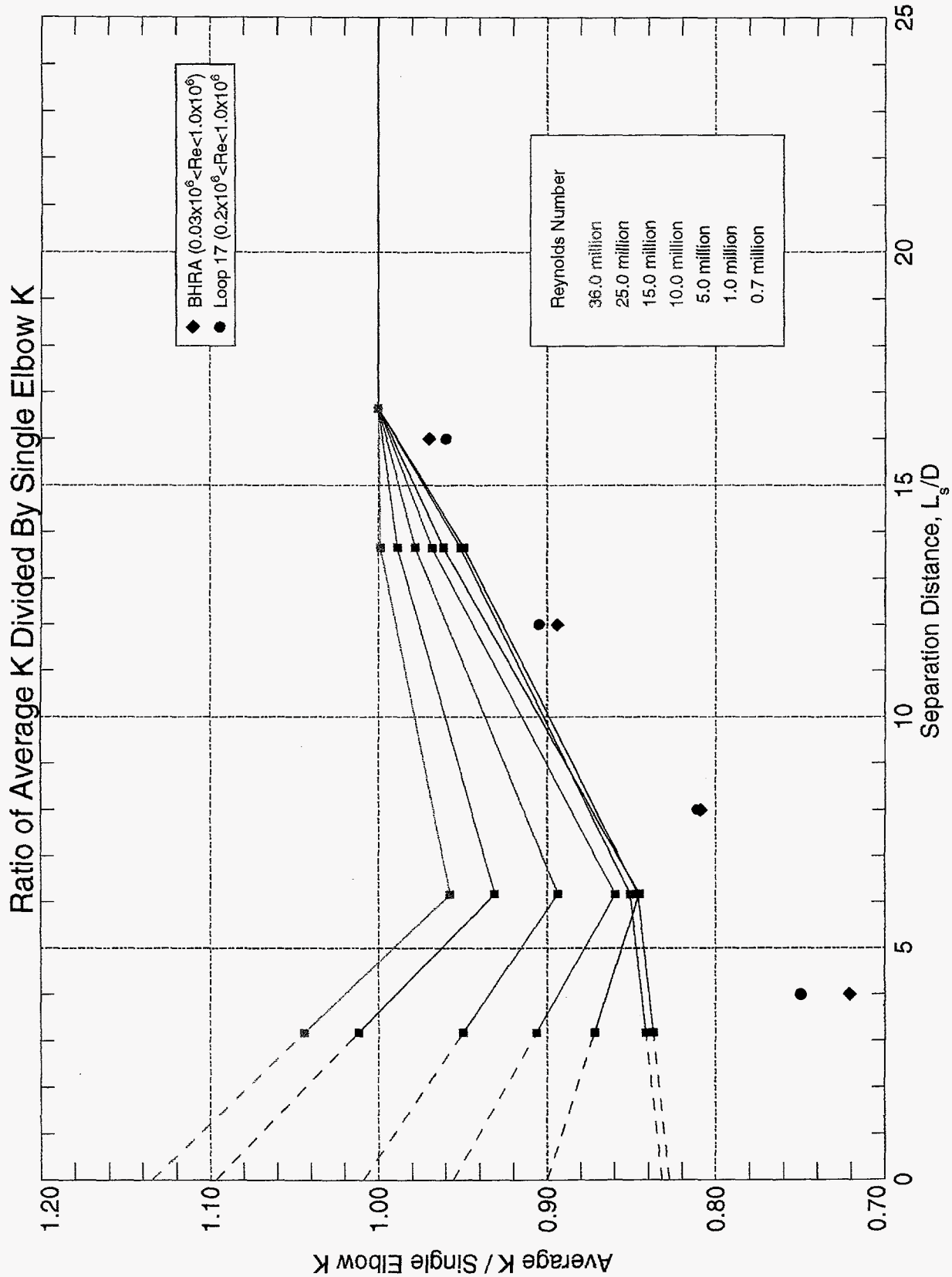
Ratio of Average K Divided By Single Elbow K
Average K / Single Elbow K
Separation Distance, L_s/D
1.20
1.10
1.00
0.90
0.80
0.70
0
5
10
15
20
25
BHRA (0.03x10^6<Re<1.0x10^6)
Loop 17 (0.2x10^6<Re<1.0x10^6
Reynolds Number
36.0 million
25.0 million
15.0 million
10.0 million
5.0 million
1.0 million
0.7 million

FIGURE 9.4

10.0 REFERENCES

(a) R. D. Coffield, et al., "Piping Elbow Irrecoverable Pressure Loss Coefficients for Moderately High Reynolds Numbers," FED-Vol. 211, pp. 19-24, 1995 ASME Fluids Engineering Conference, Hilton Head, South Carolina, August 13-18, 1995.

(b) R. D. Coffield, et al., "Irrecoverable Pressure Loss Coefficients for a Short Radius of Curvature Piping Elbow at High Reynolds Numbers," 1998 ASME Fluids Engineering Division Summer Meeting, FEDSM'98-5146, Washington, D. C., June 21-25, 1998.

(c) D. S. Miller, Internal Flow Systems, (Second Edition), published by the British Hydromechanics Research Association, 1990.

(d) I. E. Idelchik, Handbook of Hydraulic Resistance, (Second Edition, Revised and Augmented), published by Hemisphere, 1986.

(e) R. J. S. Pigott, "Losses in Pipe and Fittings," Trans. ASME, Vol. 79, 1957.

(f) Crane Technical Paper No. 410, Flow of Fluids Through Valves, Fittings, and Pipe, published by Crane Co., 1988.

(g) H. Ito, "Pressure Losses in Smooth Pipe Bends," Trans. ASME, J. Basic Eng., Vol. 82, March 1960.

(h) M. V. Zagarola, et al., "Experiments in High Reynolds Number Turbulent Pipe Flow," AIAA 96-0654, 34th Aerospace Science Meeting and Exhibit, January 15-18, 1996, Reno, NV.

(i) J. W. Daily and D. F. Harleman, Fluid Dynamics, Addison-Wesley, pp. 267-272, 1966.

(j) T. B. Drew, E. C. Koo and W. H. McAdams, "The Friction Factor for Clean Round Pipes," Transactions of the American Institute of Chemical Engineers, Vol. 28, pp. 56-72, 1932.

(k) T. T. Yah and G. E. Mattingly, "Computer Simulations of Ultrasonic Flowmeter Performance in Ideal and Non-ideal Pipe Flows," FEDSM97-3012, 1997 ASME Fluids Engineering Division Summer Meeting, Vancouver, British Columbia, June 22-26, 1997.

(l) R. D. Coffield, et al., "Irrecoverable Pressure Loss Coefficients for Two Elbows in Series With Various Orientation Angles and Separation Distances," 1997 ASME Fluids Engineering Division Summer Meeting, FEDSM97-3471, Vancouver, British Columbia, June 22-26, 1997.

THIS PAGE INTENTIONALLY BLANK